DCEF: Deep Collaborative Encoder Framework for Unsupervised Clustering

Jielei Chu, member, IEEE, Hongjun Wang, Jing Liu, Zeng Yu, Tianrui Li, Senior member, IEEE,

Abstract—Collaborative representation is a popular feature learning approach, which encoding process is assisted by variety types of information. In this paper, we propose a collaborative representation restricted Boltzmann Machine (CRRBM) for modeling binary data and a collaborative representation Gaussian restricted Boltzmann Machine (CRGRBM) for modeling realvalued data by applying a collaborative representation strategy in the encoding procedure. We utilize Locality Sensitive Hashing (LSH) to generate similar sample subsets of the instance and observed feature set simultaneously from input data. Hence, we can obtain some mini blocks, which come from the intersection of instance and observed feature subsets. Then we integrate Contrastive Divergence and Bregman Divergence methods with mini blocks to optimize our CRRBM and CRGRBM models. In their training process, the complex collaborative relationships between multiple instances and features are fused into the hidden layer encoding. Hence, these encodings have dual characteristics of concealment and cooperation. Here, we develop two deep collaborative encoder frameworks (DCEF) based on the CRRBM and CRGRBM models: one is a DCEF with Gaussian linear visible units (GDCEF) for modeling real-valued data, and the other is a DCEF with binary visible units (BDCEF) for modeling binary data. We explore the collaborative representation capability of the hidden features in every layer of the GDCEF and BDCEF framework, especially in the deepest hidden layer. The experimental results show that the GDCEF and BDCEF frameworks have more outstanding performances than the classic Autoencoder framework for unsupervised clustering task on the MSRA-MM2.0 and UCI datasets, respectively.

Index Terms—restricted Boltzmann machine; collaborative representation; Contrastive Divergence; Bregman Divergence; deep collaborative learning; unsupervised clustering.

I. INTRODUCTION

Collaborative representation (CR) originates the influential sparse representation-based classification (SRC) [1]. Approaches based on CR have achieved effective performance on classification [2]–[7], target detection [8] and face recognition [9]–[11]. They developed various collaborative strategies in the process of collaborative representation. Some studies focused on the source of superior performance of the CR [12], [13].

Recently, some works [14], [15], [16], [17], [18], [19] focus on deep collaborative learning (DCL). There are various novel deep collaborative models which have been successfully applied in practice. In [14], a novel DCL method is applied in multimodal brain development study

Jielei Chu, Hongjun Wang, Tianrui Li and Zeng Yu are with the School of Information Science and Technology, Southwest Jiaotong University, Chengdu, 611756, Sichuan, China. e-mails: {jieleichu, wanghongjun, zyu, trli}@swjtu.edu.cn.

Jing Liu is with the School of Business, Sichuan University, Sichuan, 610065, Chengdu, China. e-mail: liujing@scu.edu.cn

to address some limitations of conventional data-fusion methods. The traditional methods can not obtain complex nonlinear relationship between multiple data. So, Hu et al. [14] proposed a neural network framework to extract complex crossdata relationships. The DCL method first uses a deep neural network to represent original data, then designs a collaborative learning layer using collaborative regression to seek their correlations and link the data representation with phenotypical information. In this method, the deep learning process and collaborative learning belong to two separate processes. Zhang et al. [15] developed a novel deep architecture termed Self-and-Collaborative Attention Network (SCAN) based on the convolutional neural networks (CNN) for video person re-identification. The SCAN contains two kinds of subnetworks: a self attention subnetwork (SAN) to enhance feature representation and a collaborative attention subnetwork (CAN) to select frames from probe based on the representation of the other one. In [16], Liu et al. presented a collaborative deconvolutional neural network (C-DCNN) to jointly model two problems of single-view depth estimation and semantic segmentation in computer vision. Two deconvolutional neural networks (DCNNs) compose a C-DCNN and the depth features and semantic are combined in a unified deep network. In the training process, the depth features and semantic are integrated together to benefit each other. For face photo-sketch synthesis, Zhu et al. [17] proposed a deep collaborative framework. It has two opposite networks that can utilize the mutual interaction of two opposite mappings, which are constrained by a collaborative loss. Li et al. [18] developed a Deep Collaborative Embedding (DCE) model for social image understanding task. It incorporates the collaborative factor analysis and end-to-end learning in one unified framework for the optimal compatibility of latent space discovery and representation learning. The DCE model integrates the tag correlation, image correlation and weakly-supervised image-tag correlation simultaneously and seamlessly to collaboratively explore the rich information of social images. Xie et al. [19] proposed multi-view knowledgebased collaborative (MV-KBC) deep model for benign and malignant lung nodule classification. The model learns the characteristics of 3-D lung nodule by decomposing a 3-D nodule into nine views. A knowledge-based collaborative (KBC) submodel is constructed from each view. Then the nine KBC submodels are jointly used to classify lung nodules.

Various novel models have been proposed for deep collaborative filtering. Fu et al. [20] developed a novel deep learning method to promote the effectiveness of intelligent recommendation system by understanding the items beforehand and users. The low-dimensional vectors of items and users are learned separately in the initial stage. Then, in the prediction stage, the interaction between item and user is simulated by a feed-forward neural networks. Chae et al. [21] proposed a novel Collaborative Adversarial Autoencoders (CAAE) framework, which extends the conventional GraphGAN and IRGAN. The Autoencoder as one of the most successful DNNs is the generator and the Bayesian personalized ranking (BPR) is the discriminative model of CAAE framework. Zeng et al. [22] developed a Deep Collaborative Filtering (DCF) model, which integrated matrix completion and deep representation learning. Yue et al. [23] proposed a novel denoising method via deep fusion of convolutional and collaborative filtering for high ISO JPEG images. The proposed method fuses the strengths of collaborative and convolutional filtering using a deep CNN.

Our motivation is that how to develop some variants of RBMs to make them have the capabilities of collaborative representation. On this basis, we hope to develop some deep collaborative encoding frameworks with these variants of RBMs to explore the capabilities of deep collaborative representation. It's a known fact that classical RBM has been proven to be an excellent feature representation model [24], [25]. Then more and more researchers focus on various variants of standard RBM [26]-[36]. And many deep networks based on classical RBM and its variants are developed [37]-[44]. They have achieved great success in practical applications. However, previous studies have hardly considered CR in the process of feature learning of RBM. Then, the capability of feature representation of it is subject to some limitations. Furthermore, the deep encoding framework based on RBMs (e.g. Autoencoder) has not capability of collaborative representation.

In this paper, two types of collaborative representation RBMs are proposed to represent hidden and collaborative features: one is a collaborative representation restricted Boltzmann Machine (CRRBM) for modeling binary data and the other is a collaborative representation Gaussian restricted Boltzmann Machine (CRGRBM) for modeling real-valued data. Locality Sensitive Hashing (LSH) [45] is employed to generate similar sample subsets of the instance and observed feature set simultaneously from input data. Hence, some mini blocks are obtained, which come from the intersection of instance and observed feature subsets. Then Contrastive Divergence and Bregman Divergence methods are integrated with mini blocks to optimize our CRRBM and CRGRBM models. To extract deep hidden and collaborative features, two types of deep collaborative encoder frameworks (DCEF) based on the CRRBM and CRGRBM models are proposed: one is a DCEF with Gaussian linear visible units (GDCEF) for modeling real-valued data, and the other is a DCEF with binary visible units (BDCEF) for modeling binary data. The collaborative representation capability of the hidden features in every layer of the GDCEF and BDCEF frameworks are exploited, especially on the deepest hidden layer.

To best of our knowledge, our work is the first one to explore collaborative representation capability of RBMs by developing variants of classic RBMs and extract deep collaborative hidden features by constructing deep Collaborative Encoder Frameworks. Our major contributions of this paper are summarized as follows:

- A collaborative representation restricted Boltzmann Machine (CRRBM) and a collaborative representation Gaussian restricted Boltzmann Machine (CRGRBM) models are developed to represent hidden and collaborative features for binary and real-valued data, respectively.
- Contrastive Divergence and Bregman Divergence methods are integrated to optimize the proposed CRRBM and CRGRBM models. The hidden collaborative features of the proposed CRRBM and CRGRBM models fuse complex relationship of multi-instances and observed features (mini blocks) of the input data.
- Two novel deep Collaborative Encoder Frameworks (GD-CEF and BDCEF) based on CRRBM and CRGRBM models are proposed for exploiting deep collaborative features for unsupervised clustering. On each hidden layer of the proposed GDCEF and BDCEF, their more powerful capabilities of extracting deep collaborative features are exploited, especially on the deepest hidden layer.

The remaining of the paper is organized as follows. The theoretical background is described in Section II. Two collaborative representation RBMs are developed in Section III. A learning algorithm of CRRBM model is given in Section IV. Two deep collaborative encoder frameworks are proposed in Section V. The experimental results are shown in Section VI. Finally, our contributions are summarized in Section VII.

II. THEORETICAL BACKGROUND

A. Restricted Boltzmann Machine

1) Binary Visible Units: For classic RBMs [24], its architecture is a shallow two-layer structure, which consists of a binary visible and hidden layer. The energy function of RBMs is defined by:

$$E(\mathbf{v}, \mathbf{h}) = -\sum_{i \in visibles} a_i v_i - \sum_{j \in hiddens} b_j h_j - \sum_{i,j} v_i h_j w_{ij},$$
(1)

where \mathbf{v} and \mathbf{h} are the visible and hidden layer vectors, respectively, v_i and h_j are the binary visible and hidden units, respectively, w_{ij} is the symmetric connection weight between them, a_i and b_j are the biases of visible and hidden units, respectively.

Given a visible vector \mathbf{v} , the binary state h_j is equal to 1 with probability

$$p(h_j = 1 | \mathbf{v}) = \sigma(b_j + \sum_i v_i w_{ij}), \tag{2}$$

where $\sigma(x) = \frac{1}{1 + \exp(-x)}$, which is a logistic sigmoid function

Similarly, given a hidden vector \mathbf{h} , an unbiased sample of the binary state v_i is equal to 1 with probability

$$p(v_i = 1|\mathbf{h}) = \sigma(a_i + \sum_j h_j w_{ij}). \tag{3}$$

Because it is difficult to get an unbiased sample of $\langle v_i h_j \rangle_{model}$, Hinton proposed a faster learning algorithm by Contrastive Divergence (CD) [25], [26] method. Then the update rules of parameters is given by:

$$\Delta w_i j = \varepsilon (\langle v_i h_j \rangle_{data} - \langle v_i h_j \rangle_{recon}), \tag{4}$$

$$\Delta a_i = \varepsilon (\langle v_i \rangle_{data} - \langle v_i \rangle_{recon}), \tag{5}$$

$$\Delta b_j = \varepsilon (\langle h_j \rangle_{data} - \langle h_j \rangle_{recon}), \tag{6}$$

where ε is learning rate.

2) Gaussian Linear Visible Units: For modeling real-valued data, the binary visible units are replaced by Gaussian linear visible units. This energy function becomes:

$$E(\mathbf{v}, \mathbf{h}) = -\sum_{i \in visibles} \frac{(v_i - a_i)^2}{2\sigma_i^2} - \sum_{j \in hiddens} b_j h_j - \sum_{i,j} \frac{v_i}{\sigma_i} h_j w_{ij},$$

$$(7)$$

where σ_i is the standard deviation of the Gaussian noise for visible unit i. It is difficult to use CD method to learn the variance of the noise. In practice, we normalise the original data to have unit variance and zero mean. So, the reconstructed result of a Gaussian linear visible unit is equal to the input from hidden binary units plus the bias.

B. Encoder Framework of Autoencoder

- 1) Classic Autoencoder: The framework of Autoencoder [37] consists of a stack of RBMs, which is shown in Fig. 1 (right one). In the encoding process of the Autoencoder, the learned hidden features of one RBM are used as the input for training the next one. This layer-by-layer learning is an effective method to train the deep Autoencoder model. The processes of encoder and decoder are nonlinear transformation (sigmoid transformation).
- 2) Autoencoder with Gaussian Linear visible Units: To model real-valued data, the binary units of visible layer of Autoencoder can be replaced by Gaussian linear visible units, which is shown in Fig. 1 (left one). The training method is still a layer-by-layer learning pattern. The process of encoder is still sigmoid transformation, but the top decoder is a linear transformation.

III. THE MODEL OF COLLABORATIVE REPRESENTATION $$\operatorname{RBM}$$

The major goal of classic RBMs is to learn hidden layer features from the original data, with the connection matrix **W** serving as the mapping between the data and hidden features. In their processes of training, only the relationship between instances (rows) is usually considered. In many cases the hidden features we wish to obtain is often rather collaborative representation both of instances and features. In this work, the original data matrix is divided into many small blocks by means of Locality Sensitive Hashing (LSH) [45] method which exploits similar samples by a weak hash function. In this way, similar instances and features cluster together in relative big row and column blocks, respectively. Then, one after another

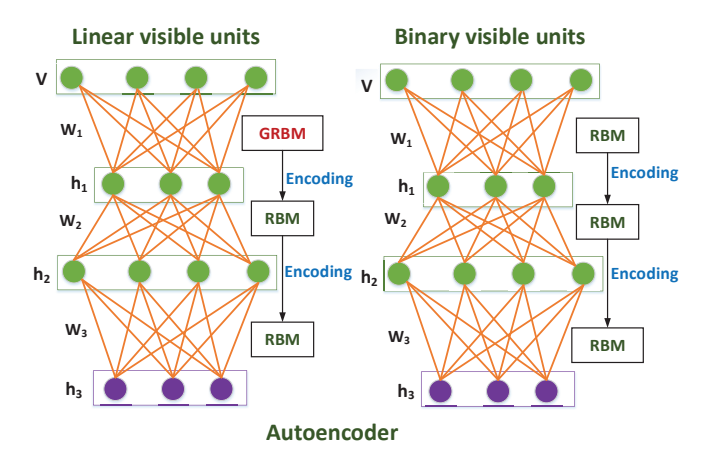


Fig. 1. Left: A deep Autoencoder with Gaussian linear visible units for real-valued data, which consists of a RBM with Gaussian linear visible units (GRBM) on the top layer and a stack of classic RBM on the down layer. The learned binary hidden features of GRBM are used as the input for training the next RBM, then the learned hidden features of this RBM are used as the input for training the following RBM in the stack. Right: A classic deep Autoencoder, which consists of a RBM stack, and the learned hidden layer features of one RBM are used as the input for training the next one.

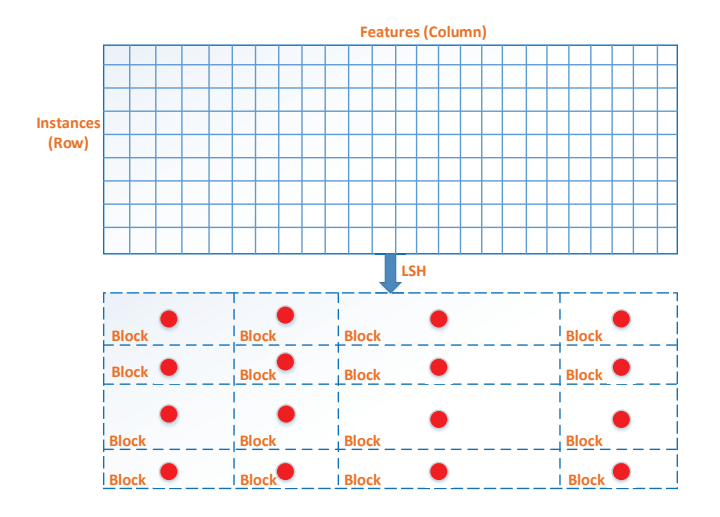


Fig. 2. Example of Block partition: the rows and columns of visible data matrix are partitioned into K(e.g.K=4) row clusters and L(e.g.L=4) column clusters by LSH. The same row and column clusters gather together and the overlaps (rows and columns) compose each block. Every red point represents the center of each block. We use dashed lines to denote the recombination matrix (virtual matrix) of the original data.

small crossed blocks with rows and columns will appear (see Fig. 2). Our expectation is that each block data possibly gather towards its own center in collaborative representation space. So, this improved RBM is called Collaborative Representation RBM (CRRBM). Supposing that the CRRBM has Gaussian linear visible units, we call it Collaborative Representation GRBM (CRGRBM). Next, the crucial problem we need to solve is that how to model the variant RBMs and obtain the update rules of the model parameters.

Let $\mathcal{D} = \{\mathbf{v}_1, \mathbf{v}_2, \cdots, \mathbf{v}_N\}$ be an original data set with N vectors and M features of each vector. The visible layer vector $\mathbf{v}_s = (v_{s1}, v_{s2}, \cdots, v_{si}, \cdots, v_{sM}), (i = 1, 2, \cdots, M, s = 1, 2, \cdots, N)$. The hidden layer vector

 $\mathbf{h}_s = (h_{s1}, h_{s2}, \cdots, h_{sj}, \cdots, h_{sM'}), (j = 1, 2, \cdots, M', s = 1, 2, \cdots, M', s)$ $(1, 2, \dots, N)$. The reconstructed visible layer vector $\mathbf{v}_s^{(r)} = \mathbf{v}_s^{(r)}$ $\begin{array}{lll} (v_{s1}^{(r)},v_{s2}^{(r)},\cdots,v_{si}^{(r)},\cdots,v_{sM}^{(r)}), (i=1,2,\cdots,M,s=1,2,\cdots,N). & \text{The reconstructed hidden layer vector } \mathbf{h}_s^{(r)} = (h_{s1}^{(r)},h_{s2}^{(r)},\cdots,h_{sj}^{(r)},\cdots,h_{sM}^{(r)}), (j=1,2,\cdots,M',s=1,2,\cdots,N). & \text{The matrix } (\mathbf{v}_1^T\mathbf{v}_2^T\cdots\mathbf{v}_N^T)^T & \text{is partitioned into} \end{array}$ K row clusters by LSH and each cluster has a serial number set of vectors \Re_k , $(k=1,2,\cdots,K)$ and $\Re_1 \cup \Re_2 \cdots \cup \Re_K =$ $\{1, 2, \cdots, N\}$). Simultaneously, the matrix is partitioned into L column clusters by LSH and each cluster has a serial number set of vectors $\ell_l, (l = 1, 2, \dots, L \text{ and } \ell_1 \cup \ell_2 \dots \cup \ell_K = 1, \dots, \ell_k =$ $\{1, 2, \cdots, M\}$). So, the matrix is divided into $K \times L$ blocks.

Based on the expectations of our collaborative representation method and the training objective of classic RBM, our novel objective function takes the form:

$$G(\mathbf{V}, \theta) = -\frac{\eta}{N} \sum_{\mathbf{v}_i} \log^{p(\mathbf{v}_i; \theta)} + \frac{(1 - \eta)}{K \times L} \left[\sum_{k=1}^K \sum_{l=1}^L \sum_{s \in \Re_k} \sum_{t \in \ell_l} d(h_{st}, u_{kl}) + \sum_{k=1}^K \sum_{l=1}^L \sum_{s \in \Re_k} \sum_{t \in \ell_l} d(h_{st}^{(r)}, u_{kl}^{(r)}) \right],$$

where $\theta = \{\mathbf{a}, \mathbf{b}, \mathbf{W}\}$ are the model parameters, η is an adjusting parameter, $d(h_{st}, u_{kl})$ and $d(h_{st}^{(r)}, u_{kl}^{(r)})$ are the Bregman divergences [46] [47] distances, which are defined as: $d(h_{st}, u_{kl}) = (h_{st} - u_{kl})^2$ and $d(h_{st}^{(r)}, u_{kl}^{(r)}) = (h_{st}^{(r)} - u_{kl}^{(r)})^2$, respectively. u_{kl} and $u_{kl}^{(r)}$ are the centers of block (\Re_k, ℓ_l) in hidden layer and reconstructed hidden layer, respectively. They take the form:

$$u_{kl} = \frac{\sum_{s \in \Re_k} \sum_{t \in \ell_l} h_{st}}{|\Re_k||\ell_l|}, u_{kl}^{(r)} = \frac{\sum_{s \in \Re_k} \sum_{t \in \ell_l} h_{st}^{(r)}}{|\Re_k||\ell_l|}.$$
 (9)

IV. THE ALGORITHM

Here, we introduce the gradient descent algorithm and an analysis of its complexity in detail.

A. Learning Algorithm

To optimize the above model by gradient descent algorithm, some variables are fixed first. Then the remaining variables are updated by an iterative method. The learning algorithm is shown in Algorithm I.

Suppose that

$$C_{data} = \sum_{k=1}^{K} \sum_{l=1}^{L} \sum_{s \in \Re_k} \sum_{t \in \ell_l} (h_{st} - u_{kl})^2,$$
 (10)

$$C_{recon} = \sum_{k=1}^{K} \sum_{l=1}^{L} \sum_{s \in \Re_{t}} \sum_{t \in l_{l}} (h_{st}^{(r)} - u_{kl}^{(r)})^{2}.$$
(11)

Using the introduced variables C_{data} and C_{recon} , the objective function have another concise equivalent form:

$$G(V, \theta) = -\frac{\eta}{N} \sum_{\mathbf{v}_i} \log^{p(\mathbf{v}_i; \theta)} + \frac{(1-\eta)}{K \times L} (C_{data} + C_{recon}).$$
(12)

The following crucial problem is that how to solve this multi-objective optimization problem. For the average loglikelihood $\frac{\eta}{N}\sum_{i}\log^{p(\mathbf{v}_{i};\theta)}$, the CD method was presented to approximately follow the gradient of two divergences $CD_n =$ $\mathrm{KL}(p_0||p_\infty) - \mathrm{KL}(p_n||p_\infty)$ to avoid enormous difficulties of the log-likelihood gradient computing. Normally, we run the Markov chain from the data distribution p_0 to p_1 (one step) in CD learning. So, the following key task is how to obtain the approximative gradient of $C_{data} + C_{recon}$.

Suppose that $J_{data} = h_{st} - u_{kl}$, $J_{recon} = h_{st}^{(r)} - u_{kl}^{(r)}$, then

$$J_{data} = h_{st} - \frac{\sum\limits_{s \in \Re_k} \sum\limits_{t \in \ell_l} h_{st}}{|\Re_k||\ell_l|} = \sigma\left(\sum\limits_{m=1}^M v_{sm} w_{mt} + b_{st}\right)$$

$$- \frac{\sum\limits_{s \in \Re_k} \sum\limits_{t \in \ell_l} \sigma\left(\sum\limits_{m=1}^M v_{sm} w_{mt} + b_{st}\right)}{|\Re_k||\ell_l|}$$

$$(13)$$

(8)

$$J_{recon} = h_{st}^{(r)} - \frac{\sum_{s \in \Re_k} \sum_{t \in \ell_l} h_{st}^{(r)}}{|\Re_k||\ell_l|} = \sigma\left(\sum_{m=1}^M v_{sm}^{(r)} w_{mt} + b_{st}^{(r)}\right)$$
$$- \frac{\sum_{s \in \Re_k} \sum_{t \in \ell_l} \sigma\left(\sum_{m=1}^M v_{sm}^{(r)} w_{mt} + b_{st}^{(r)}\right)}{|\Re_k||\ell_l|}, \tag{14}$$

where σ is a sigmoid function.

When $t = j \in \ell_l$, the partial derivative of J_{data} is given by:

$$\frac{\partial J_{data}}{\partial w_{ij}} = \frac{e^{-\left(\sum_{m=1}^{M} v_{sm} w_{mj} + b_{sj}\right)} v_{si}}{\left[1 + e^{-\left(\sum_{m=1}^{M} v_{sm} w_{mj} + b_{sj}\right)}\right]^{2}} \\
- \frac{\sum_{s \in \Re_{k}} \frac{e^{-\left(\sum_{m=1}^{M} v_{sm} w_{mj} + b_{sj}\right)} v_{si}}{\left[1 + e^{-\left(\sum_{m=1}^{M} v_{sm} w_{mj} + b_{sj}\right)}\right]^{2}}}{\left|\Re_{k}\right|} \\
= (1 - h_{sj}) h_{sj} v_{si} - \frac{\sum_{s \in \Re_{k}} (1 - h_{sj}) h_{sj} v_{si}}{\left|\Re_{k}\right|}$$
(15)

Obviously, if $t \neq j$, then $\frac{\partial J_{data}}{\partial w_{ij}} = 0$. Similarly, if $t = j \in \ell_l$, the partial derivative of J_{recon} is given by:

$$\frac{\partial J_{recon}}{\partial w_{ij}} = (1 - h_{sj}^{(r)}) h_{sj}^{(r)} v_{si}^{(r)} - \frac{\sum_{s \in \Re_k} (1 - h_{sj}^{(r)}) h_{sj}^{(r)} v_{si}^{(r)}}{|\Re_k|}$$
(16)

As for model parameter **b**, if t = j, the partial derivative takes the forms:

$$\frac{\partial J_{data}}{\partial b_{j}} = (1 - h_{sj})h_{sj} - \frac{\sum_{s \in \Re_{k}} (1 - h_{sj})h_{sj}}{|\Re_{k}|},
\frac{\partial J_{recon}}{\partial b_{j}} = (1 - h_{sj}^{(r)})h_{sj}^{(r)} - \frac{\sum_{s \in \Re_{k}} (1 - h_{sj}^{(r)})h_{sj}^{(r)}}{|\Re_{k}|}.$$
(17)

It is obvious that model parameter **a** is independent of J_{data} and J_{recon} . So, we can obtain that $\frac{\partial J_{data}}{\partial a_i} = 0$ and $\frac{\partial J_{recon}}{\partial a_i} = 0$. Then, the partial derivative of the C_{data} in terms of w_{ij} takes the form:

$$\frac{\partial C_{data}}{\partial w_{ij}} = 2 \sum_{k=1}^{K} \sum_{s \in \Re_k} \left(h_{sj} - \frac{\sum_{s \in \Re_k} h_{sj}}{|\Re_k|} \right) \left[(1 - h_{sj}) h_{sj} v_{si} - \frac{\sum_{s \in \Re_k} (1 - h_{sj}) h_{sj} v_{si}}{|\Re_k|} \right].$$
(18)

And the partial derivative of the C_{recon} in terms of w_{ij} takes the form:

$$\frac{\partial C_{recon}}{\partial w_{ij}} = 2 \sum_{k=1}^{K} \sum_{s \in \Re_{k}} \left(h_{sj}^{(r)} - \frac{\sum_{s \in \Re_{k}} h_{sj}^{(r)}}{|\Re_{k}|} \right) \left[(1 - h_{sj}^{(r)}) h_{sj}^{(r)} v_{si}^{(r)} - \frac{\sum_{s \in \Re_{k}} (1 - h_{sj}^{(r)}) h_{sj}^{(r)} v_{si}^{(r)}}{|\Re_{k}|} \right].$$
(10)

Similarly, the partial derivative of the C_{data} in terms of b_j is given by:

$$\frac{\partial C_{data}}{\partial b_j} = 2 \sum_{k=1}^K \sum_{s \in \Re_k} \left(h_{sj} - \frac{\sum_{s \in \Re_k} h_{sj}}{|\Re_k|} \right) \left[(1 - h_{sj}) h_{sj} - \frac{\sum_{s \in \Re_k} (1 - h_{sj}) h_{sj}}{|\Re_k|} \right].$$
(20)

And the partial derivative of the C_{recon} in terms of b_j is given by:

$$\frac{\partial C_{recon}}{\partial b_{j}} = 2 \sum_{k=1}^{K} \sum_{s \in \Re_{k}} \left(h_{sj}^{(r)} - \frac{\sum_{s \in \Re_{k}} h_{sj}^{(r)}}{|\Re_{k}|} \right) \left[(1 - h_{sj}^{(r)}) h_{sj}^{(r)} - \frac{\sum_{s \in \Re_{k}} (1 - h_{sj}^{(r)}) h_{sj}^{(r)}}{|\Re_{k}|} \right].$$
(21)

Combined with the CD learning with 1 step Gibbs sampling, the update rule of the proposed model parameter \mathbf{W} takes the forms:

$$w_{ij}^{(\tau+1)} = w_{ij}^{(\tau)} + \eta \varepsilon (\langle v_i h_j \rangle_{data} - \langle v_i h_j \rangle_{recon})$$

$$+ \frac{2(1-\eta)}{K \times L} \left\{ \sum_{k=1}^{K} \sum_{s \in \Re_k} \left(h_{sj} - \frac{\sum_{s \in \Re_k} h_{sj}}{|\Re_k|} \right) \left[(1-h_{sj}) h_{sj} v_{si} \right]$$

$$- \frac{\sum_{s \in \Re_k} (1-h_{sj}) h_{sj} v_{si}}{|\Re_k|} \right] + \sum_{k=1}^{K} \sum_{s \in \Re_k} \left(h_{sj}^{(r)} - \frac{\sum_{s \in \Re_k} h_{sj}^{(r)}}{|\Re_k|} \right)$$

$$\left[(1-h_{sj}^{(r)}) h_{sj}^{(r)} v_{si}^{(r)} - \frac{\sum_{s \in \Re_k} (1-h_{sj}^{(r)}) h_{sj}^{(r)} v_{si}^{(r)}}{|\Re_k|} \right] \right\},$$

$$(22)$$

where ε is learning rate, the average $< v_i h_j >_{data}$ and $< v_i h_j >_{recon}$ are computed using the sample data and

reconstructed data, respectively.

For the parameters of the biases **a** and **b**, the update rules of them take the forms:

$$a_i^{(\tau+1)} = a_i^{(\tau)} + \eta \varepsilon (\langle v_i \rangle_{data} - \langle v_i \rangle_{recon}), \qquad (23)$$

and

$$b_{j}^{(\tau+1)} = b_{j}^{(\tau)} + \eta \varepsilon (\langle h_{j} \rangle_{data} - \langle h_{j} \rangle_{recon})$$

$$+ \frac{2(1-\eta)}{K \times L} \left\{ \sum_{k=1}^{K} \sum_{s \in \Re_{k}} \left(h_{sj} - \frac{\sum_{s \in \Re_{k}} h_{sj}}{|\Re_{k}|} \right) \left[(1-h_{sj}) h_{sj} - \frac{\sum_{s \in \Re_{k}} (1-h_{sj}) h_{sj}}{|\Re_{k}|} \right] + \sum_{k=1}^{K} \sum_{s \in \Re_{k}} \left(h_{sj}^{(r)} - \frac{\sum_{s \in \Re_{k}} h_{sj}^{(r)}}{|\Re_{k}|} \right) \left[(1-h_{sj}) h_{sj}^{(r)} - \frac{\sum_{s \in \Re_{k}} (1-h_{sj}^{(r)}) h_{sj}^{(r)}}{|\Re_{k}|} \right] \right\}.$$

$$\left[(1-h_{sj}^{(r)}) h_{sj}^{(r)} - \frac{\sum_{s \in \Re_{k}} (1-h_{sj}^{(r)}) h_{sj}^{(r)}}{|\Re_{k}|} \right] \right\}.$$

$$(24)$$

Algorithm 1 Learning algorithm of CRRBM with 1 step Gibbs sampling

Input:

 \mathcal{D} : input data sets;

 \mathcal{B} : training batch sets;

 ε : learning rate;

Initialize: a, b and W.

 (\Re_k, ℓ_l) : matrix blocks of $\mathcal{D}, k \in [1, K]$ and $l \in [1, L]$;

Output:

 θ : model parameters of CRRBM.

```
while \tau not exceeding maximum iteration do
   for all training batch {\cal B} do
       Encoder: sample the states of hidden units by Eq. (2).
       Decoder: sample the reconstructed states of visible
                      units using Eq. (3).
       for all \Re_k do
              Compute \frac{\partial C_{data}}{\partial w_{ij}} using Eq. (18).

Compute \frac{\partial C_{recon}}{\partial w_{ij}} using Eq. (19).

Compute \frac{\partial C_{data}}{\partial b_j} using Eq. (20).

Compute \frac{\partial C_{recon}}{\partial b_j} using Eq. (21).
           end for
       end for
       Update parameter W using Eq. (22).
       Update parameter a using Eq. (23).
       Update parameter b using Eq. (24).
   end for
    \tau = \tau + 1.
end while
return a, b and W.
```

In the reconstruction process of CRGRBM model, a linear reconstruction method replaces the nolinear reconstruction method of CRRBM model. The steps of the learning algorithms of our CRRBM and CRGRBM models are almost

the same, except the reconstruction process. So, we omit the learning algorithm of CRGRBM model.

B. Complexity Analysis

In this subsection, we analyze the time complexity of above learning algorithm. Supposing that the input data sets $\mathcal D$ is divided into TB training batch. Then the time complexities of the encoder and decoder steps are O(TB) in each iteration. When partial derivatives $\frac{\partial C_{data}}{\partial w_{ij}},\,\frac{\partial C_{recon}}{\partial w_{ij}},\,\frac{\partial C_{data}}{\partial b_j}$ and $\frac{\partial C_{recon}}{\partial b_j}$ are calculated, they take $O(TB\times(K\times L))$ in each iteration. The complexities of update parameters $\mathbf W$, a and b are O(TB) in each iteration. Supposing that the maximum iteration is IT. Then, the time complexity of the CRRBM learning algorithm with 1 Step Gibbs sampling is $O(IT\times TB\times(K\times L)).$

V. DEEP COLLABORATIVE ENCODER FRAMEWORK

The classic RBMs and GRBMs have capabilities of hidden layer feature representation for binary and real-valued data, respectively. Moreover, our CRRBM and CRGRBM have powerful capabilities of collaborative representation of hidden features. To explore the superior collaborative representation capability of deep networks for different data, two types of deep encoder framework with three layers (see Fig. 3) are constructed with the proposed CRRBM and CRGRBM as building blocks of the deep framework.

For real-valued data, we construct a deep architecture termed as Deep Collaborative Encoder Framework with Gaussian linear visible units (GDCEF), which consists of one CR-GRBM with Gaussian linear visible units and two CRRBMs with binary visible units, as shown in Fig. 3. The learned binary features of the CRGRBM are used as the input for training the first CRRBM. Then the binary hidden features of the first CRRBM are used as the input for training the next CRRBM. The blocks for training the CRGRBM come from the original real-valued data by LSH method. However, the blocks for training the CRRBM come from the binary hidden features by LSH method.

For binary data, we construct a deep architecture termed as Deep Collaborative Encoder Framework with binary visible units (BDCEF), which consists of three CRRBMs with binary visible units, as shown in Fig. 3. The learned binary features of the CRRBM are used as the input for training the next CRRBM. The blocks for training the first CRRBM come from the original data by LSH method. The blocks for training the other CRRBMs come from the binary hidden features of the upper CRRBM by LSH method.

VI. EXPERIMENT

To validate the collaborative representation performance of the proposed GDCEF framework for real-valued data, we conducted experiments on twelve image datasets of the Microsoft Research Asia Multimedia (MSRA-MM) 2.0 [48] by unsupervised clustering. The properties of these datasets are shown in Table I. For binary data, the proposed

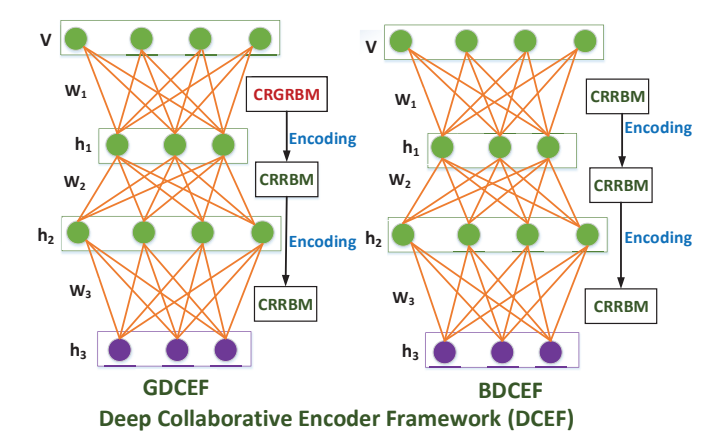


Fig. 3. Deep Collaborative Encoder Framework (DCEF). Left: A DCEF with Gaussian linear visible units (GDCEF) for real-valued data, which consists of a collaborative representation RBM with Gaussian linear visible units (CRGRBM) on the top layer and a stack of collaborative representation RBM with binary visible units (CRRBM) on the down layer. The learned binary hidden features of CRGRBM are used as the input for training the next CRRBM, then the learned hidden features of CRRBM are used as the input for training the following CRRBM in the stack. Right: A DCEF with binary visible units (BDCEF) for binary data, which consists of a CRRBM stack, and the learned hidden layer features of one CRRBM are used as the input

BDCEF framework is used to assess the collaborative representation performance by unsupervised clustering on twelve UCI datasets. The details of them are shown in Table II.

A. Experimental Setting

for training the next one.

In the following experiments, the deep Autoencoder [37] is used to compare with our GDCEF and BDCEF networks. For real-valued data, the Gaussian linear units are used in visible layer of the deep Autoencoder. For the sake of fairness in comparison, we use the same parameters of learning rate in the GDCEF and the Autoencoder. For binary data, we use classic deep Autoencoder with binary visible and hidden units to compare the capabilities of feature representation with our BDCEF framework. Similarly, we use the same parameters of learning rate in the BDCEF and the classic Autoencoder. In all experiments, the dimensionality of the data and features remain the same. The experiments are divided into three stages that are hidden layer features learning by Autoencoder, GDCEF and BDCEF frameworks, unsupervised clustering with the learned features and evaluations.

We use three popular external evaluations, e.g., accuracy [49], Jaccard index [50] and Fowlkes and Mallows Index (FMI) [51], to evaluate the performance of the proposed GDCEF and BDCEF frameworks by unsupervised clustering tasks. The accuracy [49] is an external evaluation metric, which takes the form:

$$accuracy = \frac{\sum_{i=1}^{n} \delta(s_i, map(r_i))}{n},$$
(25)

where $map(r_i)$ maps label r_i of each cluster to the equivalent label and n is the total number of instances. If x = y, then

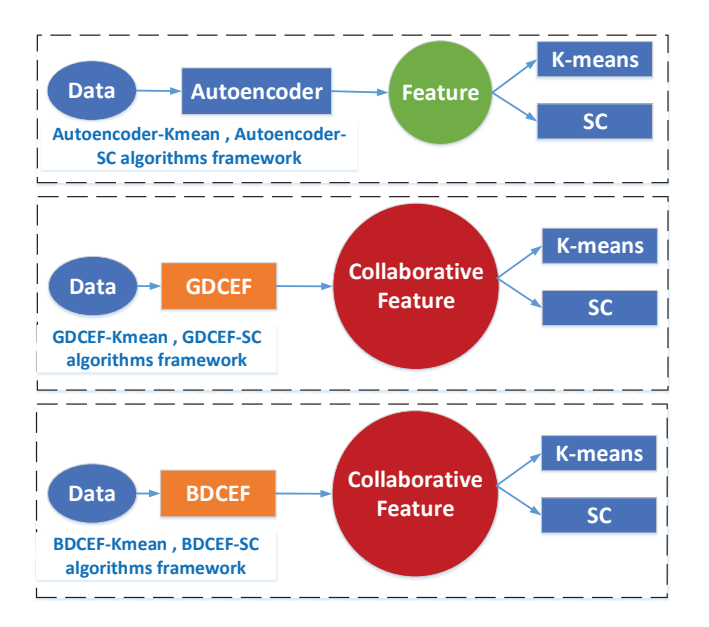


Fig. 4. The frameworks of contrast unsupervised clustering algorithms based on Autoencoder (Autoencoder-Kmeans and Autoencoder-SC algorithms), GD-CEF (GDCEF-Kmeans and GDCEF-SC algorithms) and BDCEF (BDCEF-Kmeans and BDCEF-SC algorithms) framework.

 $\delta(x,y)$ equals to 1 . Otherwise, it is zero. The Jaccard index [50] metric is defined by:

$$Jac = \frac{|A \cap B|}{|A \cup B|},\tag{26}$$

where A and B are finite sample sets and $0 \le J(A, B) \le 1$. The FMI [51] as an external evaluation metric is given by:

$$\mathbf{FMI} = \sqrt{\frac{TP}{TP + FP}} \times \frac{TP}{TP + FN},\tag{27}$$

where TP is the number of true positives, FP is the number of false positives and and FN is the number of false negatives.

In the stage of unsupervised clustering, we use separately K-means [52] and Spectral Clustering (SC) [53] algorithms to evaluate the capabilities of feature representation of Autoencoder, GDCEF and BDCEF frameworks. The hidden features of the Autoencoder are used as the input of K-means and SC, so we call these contrastive clustering algorithms Autoencoder-Kmeans and Autoencoder-SC, respectively. The algorithm frameworks of them are shown in Fig. 4. Similarly, The hidden features of the GDCEF and BDCEF are used as the input of K-means and SC, we call these clustering algorithms GDCEF-Kmeans, GDCEF-SC, BDCEF-Kmeans, BDCEF-SC, respectively. The algorithm frameworks of them are shown in Fig. 4.

B. GDCEF vs Autoencoder with Gaussian Linear Visible Units by Unsupervised Clustering

In this section, we compare the collaborative representation utility of the GDCEF framework with the Autoencoder on the MSRA-MM2.0 [48] datasets by unsupervised clustering and the experiments are duplicated ten times. In the GDCEF

 $\begin{tabular}{l} TABLE\ I \\ SUMMARY\ OF\ THE\ EXPERIMENT\ DATASETS\ I. \end{tabular}$

No.	Dataset	classes	Instances	features
1	banner	3	860	892
2	beret	3	876	892
3	bugat	3	882	892
4	bugatti	3	882	892
5	building	3	911	892
6	vista	3	799	899
7	vistawallpaper	3	799	899
8	voituretuning	3	879	899
9	water	3	922	899
10	weddingring	3	897	899
11	wing	3	856	899
12	worldmap	3	935	899

No.	Dataset	classes	Instances	features
1	balance	3	625	4
2	biodegradation	2	1055	41
3	car	4	1728	6
4	Climate Model	2	540	18
5	cred (Credit Approval)	2	690	15
6	dermatology	6	366	34
7	Haberman Survival	2	306	3
8	ILPD(Indian Liver Patient)	2	583	8
9	Kdd (1999 partial data)	3	1280	41
10	OLD (Ozone Level Detection)	2	2534	72
11	` parkinsons	2	195	22
12	secom	2	1567	590

framework, the visible units are Gaussian linear visible units, so we use the same Gaussian linear units in the visible layer of the Autoencoder.

Fig. 5 shows the comparison of clustering accuracies among the original data, the deepest layer hidden features of the Autoencoder and GDCEF framework on twelve image data sets using K-means and SC algorithms. For every data set on Table I, whether by K-means or SC clustering algorithms, the hidden features of GDCEF shows better performance than the hidden features of Autoencoder. In particular, the data sets of banner, beret, building, vista and voituretuning show outstanding performance on our GDCEF framework for the K-means algorithm. For the SC algorithm, the data sets of banner, bugat, bugatti, building, voituretuning, wing and worldmap show excellent performance on the proposed GDCEF framework. From the results of contrast experiments, we are assured that our GDCEF framework has more powerful capability of collaborative representation than the Autoencoder with Gaussian linear visible units which has not any collaborative representation strategy.

Fig. 6 shows the comparison of average clustering accuracies of all data sets in Table I in every layer (visible layer data, the first layer hidden features, the second layer hidden features and the third layer hidden features) of Autoencoder and GDCEF by K-means and SC algorithms. For K-means algorithm, the average accuracies are 0.4419, 0.4029, 0.4110 and 0.4087 from the visible to the deepest layer of the Autoen-

coder, respectively. There is little change of performance in all hidden layers, furthermore, they show worse performance than the visible layer. However, the average accuracies are greatly raised to 0.5728, 0.5754 and 0.5987 from the first to the deepest hidden layer of our GDCEF framework by means of collaborative encoding strategy, respectively. For SC algorithm, the average accuracies are 0.4058, 0.4820, 0.3794 and 0.3542 from the visible to the deepest layer of the Autoencoder, respectively. It's obvious that the first hidden layer shows better performance than the visible layer. Unfortunately, the performance of the Autoencoder gradually declines as the layer increases. As shown in Fig. 6, the average accuracies from the first to the deepest hidden layer are 0.4386, 0.4663 and 0.6330, respectively. Although the average accuracy of the first hidden layer of GDCEF is worse than the Autoencoder, the performance increases significantly as hidden layer increases and the accuracy is eventually increased by 22.72%.

The detailed results of the clustering accuracies and variances on the GDCEF framework (the deepest hidden layer) as shown in Table III. The inputs of the K-means and SC algorithms are the original data. The Autoencoder-Kmeans and Autoencoder-SC algorithms use the deepest hidden layer (the third hidden layer) features of the Autoencoder as the inputs. Similarly, the GDCEF-Kmeans and GDCEF-SC algorithms use the deepest hidden layer (the third hidden layer) features of the GDCEF framework as the inputs. The average accuracies of GDCEF-Kmeans and GDCEF-SC algorithms are 0.5987 and 0.6330, respectively, which are 19% and 27.88% higher than Autoencoder-Kmeans and the Autoencoder-SC algorithms. Furthermore, they are 15.68% and 22.72% higher than K-means and SC algorithms. The GDCEF-Kmeans algorithm shows the best performance on the data sets of the banner, beret, building, vista, voituretuning and wing. Moreover, GDCEF-SC algorithm shows the best performance on the data sets of the bugat, bugatti, vistawallpaper, water, weddingring and worldmap. As a whole, our GDCEF framework has excellent capability of collaborative representation.

To prove the collaborative representation ability of our GDCEF framework in more ways, Tables IV and V show the results of the other two evaluating metrics of the Jaccard index and FMI. On the whole, the average Jaccard index of K-means, SC, Autoencoder-Kmeans and Autoencoder-SC algorithms are 0.4040, 0.2683, 0.2793 and 0.2563, respectively. But, the GDCEF-Kmeans and GDCEF-SC algorithms raise the average Jaccard index to 0.4424 and 0.5032, respectively. In Table V, the average FMI of K-means, SC, Autoencoder-Kmeans and Autoencoder-SC algorithms are 0.5715, 0.4354, 0.4444 and 0.4206, respectively. However, the GDCEF-Kmeans and GDCEF-SC algorithms raise the average FMI to 0.6168 and 0.6864, respectively. Almost all data sets in Table I show the best performance on the GDCEF framework by the evaluations of Jaccard index and FMI except the data set of bugat.

From all above results of the experiments, our GDCEF shows outstanding capability of collaborative representation.

C. BDCEF vs Autoencoder with Binary Visible Units by Unsupervised Clustering

Here, we evaluate the collaborative representation performance on the twelve UCI datasets by unsupervised clustering in terms of the accuracy, Jaccard index and FMI evaluation metrics. We compare our BDCEF framework with the Autoencoder, which has binary visible units.

Results for the comparison of clustering accuracies among the original data, the deepest hidden layer features of the Autoencoder and BDCEF framework by K-means and SC algorithms are shown on Fig. 7. More detailed comparisons of K-means, SC, Autoencoder-Kmeans, Autoencoder-SC, BDCEF-Kmeans and BDCEF-SC algorithms are shown in Table VI. As a whole, the average accuracies of Autoencoder-Kmeans and Autoencoder-SC algorithms without collaborative strategy are 0.5951 and 0.6234, respectively. But, the average accuracies of BDCEF-Kmeans and BDCEF-SC algorithms based on our BDCEF framework are raised to 0.7122 and 0.7014, respectively. So, the collaborative representation strategy improves the performance of BDCEF-Kmeans and BDCEF-SC algorithms by 11.71% and 7.8%. For each data set in Table II, the BDCEF-Kmeans algorithm shows outstanding performance than other comparison algorithms on the data sets of balance, biodegradation, cred, dermatology, ILDP, Kdd, OLD, parkinsons and secom. The accuracies of them are 0.6224, 0.6673, 0.6841, 0.4754, 0.8136, 0.9877, 0.9369, 0.8051 and 0.9336, respectively. Another algorithm based on our BDCEF framework is BDCEF-SC, which shows excellent performance than other comparison algorithms on the data sets of car, ClimateModel and HabermanSurvival. The accuracies of them are 0.6985, 0.9111 and 0.7255, respectively.

To explore the effect of collaborative representation strategy in every hidden layer of our BDCEF framework, the comparison of average clustering accuracies of all data sets in Table II are shown on the Fig. 8. The average accuracies of the first hidden layer, the second hidden layer and the third hidden layer are 0.6476, 0.6691 and 0.7122 by K-means algorithm, respectively. As the hidden layers of our BDCEF framework increase, the performances of them are increased by 7.35%, 9.5% and 13.81%, respectively. For SC algorithm, the average accuracies of the first, second and third hidden layer are 0.6837, 0.6940 and 0.7014, respectively. Similarly, as the hidden layer of our BDCEF framework increases, the performances of them are increased by 14.02%, 15.05% and 15.79%, respectively. But, without the help of a collaborative representation strategy, the average accuracies of the Kmeans algorithm in the first, second and third layer of the Autoencoder drop to 0.5864, 0.5986 and 0.5951, respectively, in contrast with our BDCEF framework. Similarly, the average accuracies of the SC algorithm in the first, second and third layer of the Autoencoder drop to 0.6584, 0.6229 and 0.6234, respectively.

Table VII shows the results of Jaccard index on UCI data sets. For BDCEF-Kmeans algorithm based on our BDCEF framework, the data sets of dermatology, ILPD, Kdd, OLD and secom show the best performance. The Jaccard indices of them are 0.3555, 0.5817, 0.9806, 0.8816 and 0.7634,

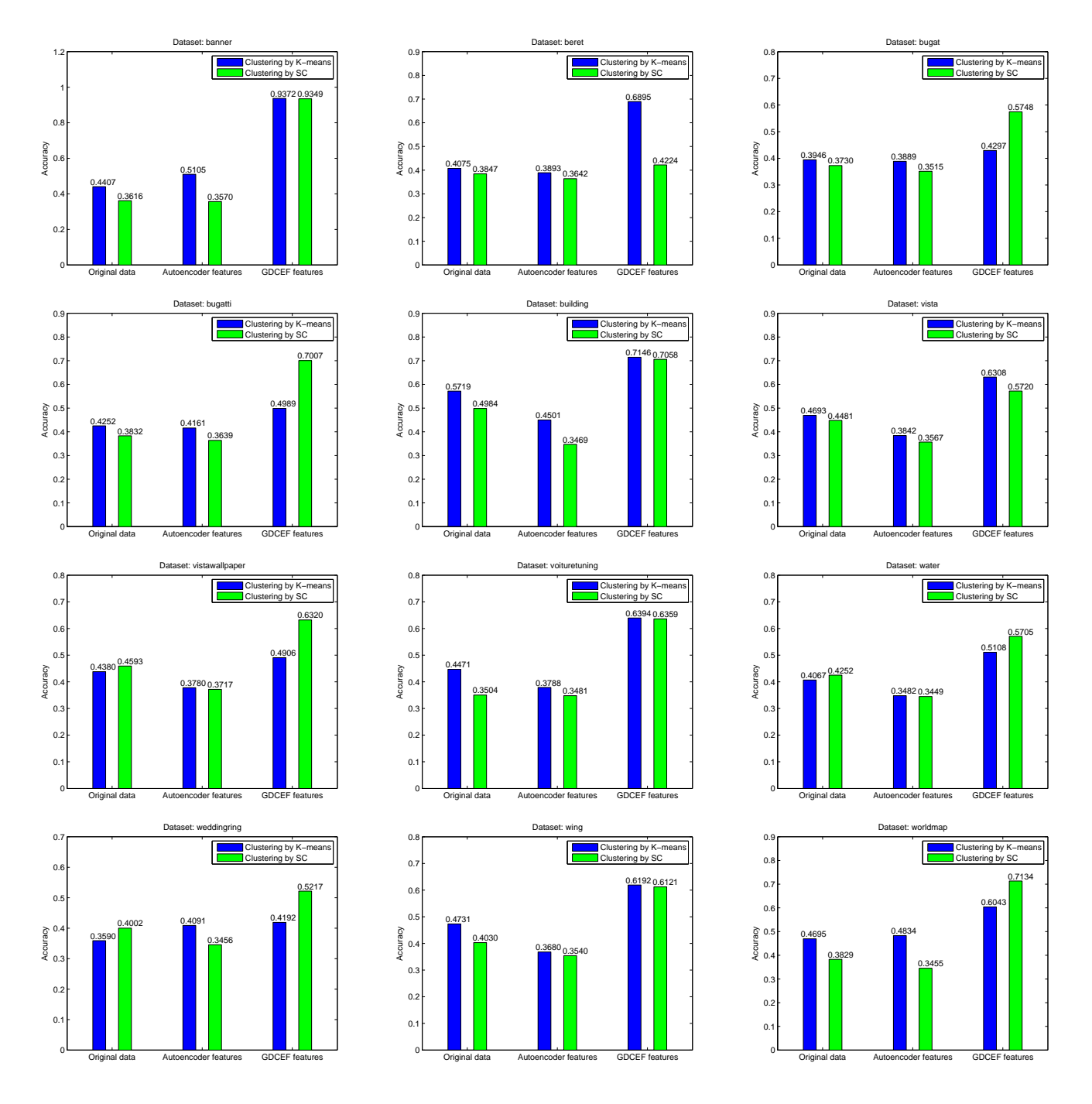


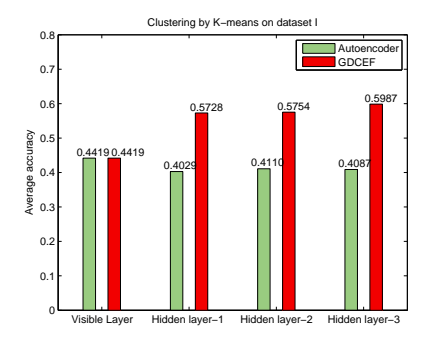
Fig. 5. The comparison of clustering accuracies among the original data, the deepest hidden features of Autoencoder and GDCEF by K-means and SC clustering algorithms. In this Autoencoder deep networks, the visible layer units are Gaussian linear units.

respectively. For BDCEF-SC algorithm based on the proposed BDCEF framework, the data sets of balance, biodegradation, car, ClimateModel, cred and parkinsons show the best performance. The Jaccard indices of them are 0.4285, 0.5525, 0.5408, 0.8370, 0.4666 and 0.6319, respectively. Only one data set (HabermanSurvival) shows the best performance in Autoencoder-Kmeans algorithm.

Table VIII shows the results of FMI on UCI data sets. For BDCEF-Kmeans algorithm, there are five data sets (dermatology, ILPD, Kdd, OLD and secom) show the best performance. The FMI of them are 0.5249, 0.7592, 0.9853, 0.9390 and

0.8658, respectively. For BDCEF-SC algorithm, there are six other data sets (balance, biodegradation, car, ClimateModel, cred and parkinsons) show best performance. Only one data set (HabermanSurvival) shows outstanding performance in Autoencoder-Kmeans algorithm.

From above the results of comparison experiments, all three selected evaluation metrics show better performance on our BDCEF framework than classic Autoencoder framework in the capability of the features representation.



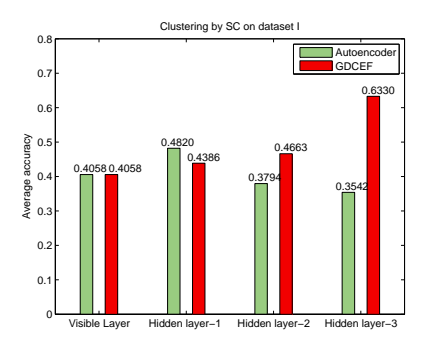


Fig. 6. The comparison of average clustering accuracies of all data sets in Table I among the original data, the first hidden layer features, the second hidden layer features and the third hidden layer features of Autoencoder and GDCEF by K-means and SC clustering algorithms. In this Autoencoder deep networks, the visible layer units are Gaussian linear units.

TABLE III THE ACCURACIES AND VARIANCES OF CLUSTERING BY K-MEANS AND SC ALGORITHMS WITH THE ORIGINAL DATA, AUTOENCODER-KMEANS AND AUTOENCODER-SC ALGORITHMS WITH THE DEEPEST HIDDEN LAYER FEATURES OF THE AUTOENCODER, GDCEF-KMEANS AND GDCEF-SC ALGORITHMS WITH THE DEEPEST HIDDEN LAYER FEATURES OF THE GDCEF FRAMEWORK (DATASET I).

Dataset	K-means	SC	Autoencoder-Kmeans	Autoencoder-SC	GDCEF-Kmeans	GDCEF-SC
banner	0.4407 ± 0.0006	0.3616 ± 0.0000	0.5105 ± 0.0004	0.3570 ± 0.0000	0.9372 ± 0.0046	0.9349 ± 0.0089
beret	0.4075 ± 0.0011	0.3847 ± 0.0001	0.3893 ± 0.0018	0.3642 ± 0.0001	0.6895 ± 0.0132	0.4224 ± 0.0112
bugat	0.3946 ± 0.0003	0.3730 ± 0.0001	0.3889 ± 0.0038	0.3515 ± 0.0000	0.4297 ± 0.0004	0.5748 ± 0.0117
bugatti	0.4252 ± 0.0007	0.3832 ± 0.0000	$0.4161\pm\ 0.0010$	0.3639 ± 0.0002	0.4989 ± 0.0028	0.7007 ± 0.0089
building	0.5719 ± 0.0021	0.4984 ± 0.0009	0.4501 ± 0.0013	0.3469 ± 0.0001	0.7146 ± 0.0000	0.7058 ± 0.0026
vista	0.4693 ± 0.0001	0.4481 ± 0.0003	0.3842 ± 0.0006	0.3567 ± 0.0001	0.6308 ± 0.0015	0.5720 ± 0.0068
vistawallpaper	0.4380 ± 0.0001	0.4593 ± 0.0001	0.3780 ± 0.0008	0.3717 ± 0.0002	0.4906 ± 0.0008	0.6320 ± 0.0054
voituretuning	0.4471 ± 0.0005	0.3504 ± 0.0000	0.3788 ± 0.0013	0.3481 ± 0.0001	0.6394 ± 0.0139	0.6359 ± 0.0025
water	0.4067 ± 0.0001	0.4252 ± 0.0000	0.3482 ± 0.0009	0.3449 ± 0.0001	0.5108 ± 0.0014	0.5705 ± 0.0044
weddingring	0.3590 ± 0.0004	0.4002 ± 0.0004	0.4091 ± 0.0010	0.3456 ± 0.0001	0.4192 ± 0.0061	0.5217 ± 0.0024
wing	0.4731 ± 0.0016	0.4030 ± 0.0004	0.3680 ± 0.0010	0.3540 ± 0.0001	0.6192 ± 0.0053	0.6121 ± 0.0046
worldmap	0.4695 ± 0.0021	0.3829 ± 0.0000	$0.4834 \pm\ 0.0020$	0.3455±0.0001	0.6043 ± 0.0030	0.7134 ± 0.0081
Average	0.4419	0.4058	0.4087	0.3542	0.5987	0.6330

TABLE IV

THE JACCARD INDEX OF CLUSTERING BY K-MEANS AND SC ALGORITHMS WITH THE ORIGINAL DATA, AUTOENCODER-KMEANS AND AUTOENCODER-SC ALGORITHMS WITH THE DEEPEST HIDDEN LAYER FEATURES OF THE AUTOENCODER, GDCEF-KMEANS AND GDCEF-SC ALGORITHMS WITH THE DEEPEST HIDDEN LAYER FEATURES OF THE GDCEF FRAMEWORK (DATASET I).

Dataset	K-means	SC	Autoencoder-Kmeans	Autoencoder-SC	GDCEF-Kmeans	GDCEF-SC
banner	0.6898	0.3197	0.3720	0.3192	0.8820	0.8779
beret	0.3573	0.2622	0.2825	0.2633	0.5348	0.5328
bugat	0.5081	0.2660	0.2668	0.2600	0.2801	0.4000
bugatti	0.5081	0.2653	0.2774	0.2606	0.3194	0.5420
building	0.3489	0.2961	0.3070	0.2629	0.5574	0.5470
vista	0.3301	0.2757	0.2582	0.2435	0.4738	0.4120
vistawallpaper	0.3301	0.2808	0.2796	0.2432	0.2714	0.4736
voituretuning	0.3022	0.2444	0.2515	0.2435	0.4760	0.4709
water	0.3081	0.2411	0.2321	0.2321	0.3561	0.4351
weddingring	0.2551	0.2421	0.2615	0.2393	0.2574	0.3274
wing	0.3986	0.2519	0.2491	0.2430	0.4714	0.4598
worldmap	0.5110	0.2744	0.3145	0.2647	0.4290	0.5602
Average	0.4040	0.2683	0.2793	0.2563	0.4424	0.5032

VII. CONCLUSIONS

In this work, two novel variants of collaborative representation RBM (CRRBM and CRGRBM) were presented for modeling binary and real-valued input data, respectively. On these bases, two novel deep collaborative encoding framework (GDCEF and BDCEF) were proposed that target (1) real-valued data and (2) binary data. We used the GDCEF and BDCEF framework to show how our collaborative strategy can yield superior performance in the feature representation process. The Autoencoder with Gaussian linear visible units was used to compare our GDCEF for unsupervised clus-

tering on the MSRA-MM2.0 datasets. Another Autoencoder with binary visible units was used to compare our BDCEF for unsupervised clustering on UCI datasets. In the contrast experiments, we compared not only the deepest layer of Autoencoder, GDCEF and BDCEF, but also the performance of every layer (visible layer, the first hidden layer, the second hidden layer and the third hidden layer). The GDCEF and BDCEF frameworks showed fairly competitive results without any fine-tuning of the model parameters for clustering tasks on the twelve image data sets and UCI data sets, respectively. In the future work, we will study how many hidden layers

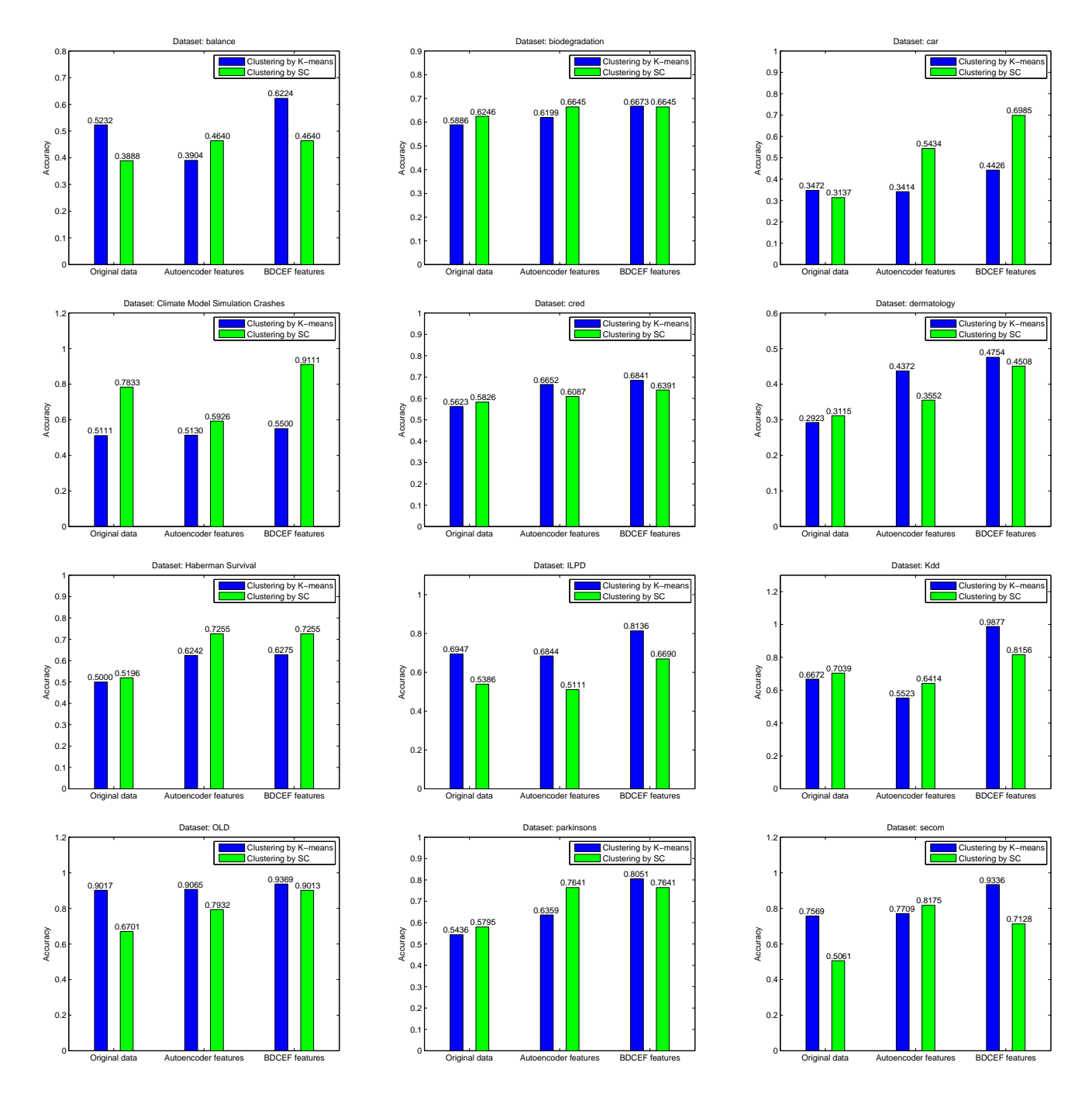


Fig. 7. The comparison of clustering accuracies among the original data, the deepest hidden features of Autoencoder and BDCEF by K-means and SC clustering algorithms. In this Autoencoder deep networks, the visible layer units are binary units.

and dimensions would result in further improvements in performance of the deep collaborative encoding framework.

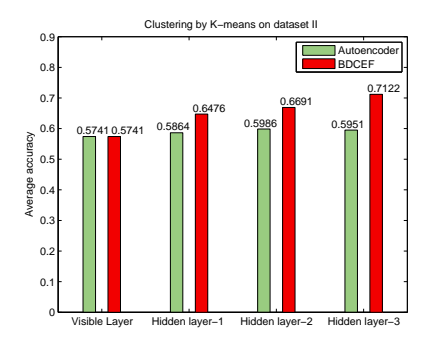
VIII. ACKNOWLEDGEMENT

This work were partially supported by the National Science Foundation of China (Nos. 61773324, 61573292, 61876158) and Sichuan Science and Technology Program (2019YFS0432).

REFERENCES

[1] J. Wright, A. Y. Yang, A. Ganesh, S. S. Sastry, and Y. Ma, "Robust face recognition via sparse representation," *IEEE Transactions on Pattern*

- Analysis and Machine Intelligence, vol. 31, no. 2, pp. 210-227, Feb 2009.
- [2] C. Zheng and N. Wang, "Collaborative representation with k-nearest classes for classification," *Pattern Recognition Letters*, vol. 117, pp. 30 – 36, 2019.
- [3] W. Li, Q. Du, and M. Xiong, "Kernel collaborative representation with tikhonov regularization for hyperspectral image classification," *IEEE Geoscience and Remote Sensing Letters*, vol. 12, no. 1, pp. 48–52, Jan 2015.
- [4] X. Chen, S. Li, and J. Peng, "Hyperspectral imagery classification with multiple regularized collaborative representations," *IEEE Geoscience* and Remote Sensing Letters, vol. 14, no. 7, pp. 1121–1125, July 2017.
- [5] J. Yang and J. Qian, "Hyperspectral image classification via multiscale joint collaborative representation with locally adaptive dictionary," *IEEE*



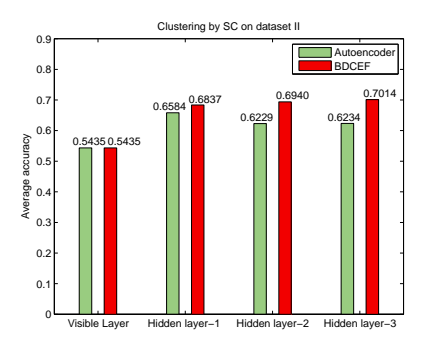


Fig. 8. The comparison of average clustering accuracies of all data sets in Table II among the original data, the first hidden layer features, the second hidden layer features and the third hidden layer features of Autoencoder and BDCEF by K-means and SC clustering algorithms. In this Autoencoder deep networks, the visible layer units are binary units.

TABLE V

THE FMI OF CLUSTERING BY K-MEANS AND SC ALGORITHMS WITH THE ORIGINAL DATA, AUTOENCODER-KMEANS AND AUTOENCODER-SC ALGORITHMS WITH THE DEEPEST HIDDEN LAYER FEATURES OF THE AUTOENCODER, GDCEF-KMEANS AND GDCEF-SC ALGORITHMS WITH THE DEEPEST HIDDEN LAYER FEATURES OF THE GDCEF FRAMEWORK (DATASET I).

Dataset	K-means	SC	Autoencoder-Kmeans	Autoencoder-SC	GDCEF-Kmeans	GDCEF-SC
banner	0.8190	0.5423	0.5876	0.5424	0.9392	0.9367
beret	0.5267	0.4373	0.4488	0.4285	0.7313	0.7288
bugat	0.6893	0.4322	0.4322	0.4294	0.4469	0.5715
bugatti	0.6893	0.4311	0.4430	0.4259	0.4902	0.7279
building	0.5190	0.4712	0.4765	0.4303	0.7466	0.7353
vista	0.4963	0.4386	0.4143	0.3979	0.6870	0.6028
vistawallpaper	0.4963	0.4442	0.4380	0.3975	0.4321	0.6865
voituretuning	0.4644	0.3990	0.4065	0.3979	0.6899	0.6808
water	0.4731	0.3920	0.3802	0.3803	0.5344	0.6585
weddingring	0.4093	0.3949	0.4167	0.3914	0.4133	0.4933
wing	0.5861	0.4079	0.4038	0.3969	0.6866	0.6692
worldmap	0.6896	0.4437	0.4849	0.4333	0.6043	0.7460
Average	0.5715	0.4354	0.4444	0.4206	0.6168	0.6864

TABLE VI

THE ACCURACIES AND VARIANCES OF CLUSTERING BY K-MEANS AND SC ALGORITHMS WITH THE ORIGINAL DATA, AUTOENCODER-KMEANS AND AUTOENCODER-SC ALGORITHMS WITH THE DEEPEST HIDDEN LAYER FEATURES OF THE AUTOENCODER, BDCEF-KMEANS AND BDCEF-SC ALGORITHMS WITH THE DEEPEST HIDDEN LAYER FEATURES OF THE BDCEF FRAMEWORK (DATASET II).

Dataset	K-means	SC	Autoencoder-Kmeans	Autoencoder-SC	BDCEF-Kmeans	BDCEF-SC
balance	0.5232 ± 0.0000	0.3888 ± 0.0000	0.3904 ± 0.0000	0.4640 ± 0.0001	$0.6224{\pm}0.0001$	0.4640 ± 0.0003
biodegradation	0.5886 ± 0.0000	0.6246 ± 0.0000	0.6199 ± 0.0002	0.6645 ± 0.0000	0.6673 ± 0.0004	0.6645 ± 0.0002
car	0.3472 ± 0.0000	0.3137 ± 0.0000	0.3414 ± 0.0000	0.5434 ± 0.0000	0.4426 ± 0.0001	0.6985 ± 0.0002
ClimateModel	0.5111 ± 0.0009	0.7833 ± 0.0000	0.5130 ± 0.0001	0.5926 ± 0.0003	0.5500 ± 0.0004	0.9111 ± 0.0011
cred	0.5623 ± 0.0000	0.5826 ± 0.0012	0.6652 ± 0.0014	0.6087 ± 0.0016	0.6841 ± 0.0026	0.6391 ± 0.0021
dermatology	0.2923 ± 0.0005	0.3115 ± 0.0000	0.4372 ± 0.0010	0.3552 ± 0.0007	0.4754 ± 0.0005	0.4508 ± 0.0004
HabermanSurvival	0.5000 ± 0.0001	0.5196 ± 0.0000	$0.6242 \pm\ 0.0009$	0.7255 ± 0.0000	0.6275 ± 0.0012	0.7255 ± 0.0007
ILPD	0.6974 ± 0.0000	0.5386 ± 0.0000	0.6844 ± 0.0001	0.5111 ± 0.0000	0.8136 ± 0.0001	0.6690 ± 0.0000
Kdd	0.6672 ± 0.0000	0.7039 ± 0.0000	0.5523 ± 0.0000	0.6414 ± 0.0002	0.9877 ± 0.0007	0.8156 ± 0.0005
OLD	0.9017 ± 0.0000	0.6701 ± 0.0000	0.9065 ± 0.0002	0.7932 ± 0.0001	0.9369 ± 0.0002	0.9013 ± 0.0001
parkinsons	0.5436 ± 0.0000	0.5795 ± 0.0001	0.6359 ± 0.0002	0.7641 ± 0.0000	0.8051 ± 0.0003	0.7641 ± 0.0000
secom	0.7569 ± 0.0000	0.5061 ± 0.0001	0.7709 ± 0.0006	0.8175 ± 0.0002	$0.9336 {\pm} 0.0003$	0.7128 ± 0.0004
Average	0.5741	0.5435	0.5951	0.6234	0.7122	0.7014

Geoscience and Remote Sensing Letters, vol. 15, no. 1, pp. 112–116, Jan 2018.

- [6] Y. Ma, C. Li, H. Li, X. Mei, and J. Ma, "Hyperspectral image classification with discriminative kernel collaborative representation and tikhonov regularization," *IEEE Geoscience and Remote Sensing Letters*, vol. 15, no. 4, pp. 587–591, April 2018.
- [7] P. Du, L. Gan, J. Xia, and D. Wang, "Multikernel adaptive collaborative representation for hyperspectral image classification," *IEEE Transactions* on Geoscience and Remote Sensing, vol. 56, no. 8, pp. 4664–4677, Aug 2018.
- [8] W. Li, Q. Du, and B. Zhang, "Combined sparse and collaborative representation for hyperspectral target detection," *Pattern Recognition*, vol. 48, no. 12, pp. 3904–3916, 2015.
- [9] J. Feng, X. Ma, and W. Zhuang, "Collaborative representation bayesian face recognition," Science China Information Sciences, vol. 60, no. 4,

- p. 048101, Dec 2016.
- [10] J. Lai and X. Jiang, "Class-wise sparse and collaborative patch representation for face recognition," *IEEE Trans Image Process*, vol. 25, no. 7, pp. 3261–3272, 2016.
- [11] J. Gou, L. Wang, Z. Yi, J. Lv, Q. Mao, and Y. Yuan, "A new discriminative collaborative neighbor representation method for robust face recognition," *IEEE Access*, vol. 6, pp. 74713–74727, Nov 2018.
- [12] W. Deng, J. Hu, and J. Guo, "Face recognition via collaborative representation: Its discriminant nature and superposed representation," *IEEE Transactions on Pattern Analysis and Machine Intelligence*, vol. 40, no. 10, pp. 2513–2521, Oct 2018.
- [13] N. Akhtar, F. Shafait, and A. Mian, "Efficient classification with sparsity augmented collaborative representation," *Pattern Recognition*, vol. 65, no. Complete, pp. 136–145, 2017.
- [14] W. Hu, B. Cai, A. Zhang, V. D. Calhoun, and Y. Wang, "Deep

TABLE VII

THE JACCARD INDEX OF CLUSTERING BY K-MEANS AND SC ALGORITHMS WITH THE ORIGINAL DATA, AUTOENCODER-KMEANS AND AUTOENCODER-SC ALGORITHMS WITH THE DEEPEST HIDDEN LAYER FEATURES OF THE AUTOENCODER, BDCEF-KMEANS AND BDCEF-SC ALGORITHMS WITH THE DEEPEST HIDDEN LAYER FEATURES OF THE BDCEF FRAMEWORK (DATASET II).

Dataset	K-means	SC	Autoencoder-Kmeans	Autoencoder-SC	BDCEF-Kmeans	BDCEF-SC
balance	0.3354	0.2387	0.2683	0.4285	0.2488	0.4285
biodegradation	0.3875	0.5147	0.3893	0.5506	0.3898	0.5525
car	0.3050	0.2221	0.2125	0.4204	0.2143	0.5408
ClimateModel	0.4957	0.6473	0.4573	0.4719	0.4601	0.8370
cred	0.4016	0.3796	0.3934	0.4499	0.4397	0.4666
dermatology	0.1654	0.1370	0.2239	0.2082	0.3555	0.1987
HabermanSurvival	0.4224	0.3787	0.6081	0.5983	0.4324	0.5983
ILPD	0.5634	0.4307	0.4305	0.4751	0.5817	0.4164
Kdd	0.5644	0.4953	0.4266	0.5492	0.9806	0.5707
OLD	0.8215	0.5374	0.8215	0.4961	0.8816	0.7560
parkinsons	0.5811	0.4134	0.4103	0.6319	0.4103	0.6319
secom	0.5265	0.4670	0.5766	0.6383	0.7634	0.4875
Average	0.4642	0.4054	0.4344	0.4932	0.5141	0.5404

TABLE VIII

THE FMI OF CLUSTERING BY K-MEANS AND SC ALGORITHMS WITH THE ORIGINAL DATA, AUTOENCODER-KMEANS AND AUTOENCODER-SC ALGORITHMS WITH THE DEEPEST HIDDEN LAYER (THE THIRD HIDDEN LAYER) FEATURES OF THE AUTOENCODER, BDCEF-KMEANS AND BDCEF-SC ALGORITHMS WITH THE DEEPEST HIDDEN LAYER FEATURES OF THE BDCEF FRAMEWORK (DATASET II).

Dataset	K-means	SC	Autoencoder-Kmeans	Autoencoder-SC	BDCEF-Kmeans	BDCEF-SC
balance	0.5024	0.3885	0.4263	0.6533	0.4010	0.6533
biodegradation	0.5586	0.7046	0.5551	0.7431	0.5615	0.7429
car	0.4814	0.3841	0.3743	0.5977	0.3798	0.7346
ClimateModel	0.6784	0.7874	0.6491	0.6626	0.6527	0.9140
cred	0.5731	0.5504	0.5647	0.6273	0.6137	0.6494
dermatology	0.2839	0.2412	0.3659	0.4452	0.5249	0.4398
HabermanSurvival	0.5940	0.5519	0.7778	0.7699	0.6038	0.7699
ILPD	0.7412	0.6030	0.6026	0.6487	0.7592	0.5898
Kdd	0.7490	0.6669	0.6097	0.7308	0.9853	0.7282
OLD	0.9023	0.7134	0.9023	0.6864	0.9390	0.8612
parkinsons	0.7453	0.5861	0.5843	0.7938	0.5839	0.7938
secom	0.7059	0.6618	0.7419	0.7844	0.8658	0.6771
Average	0.6263	0.5700	0.5962	0.6784	0.6567	0.7128

- collaborative learning with application to multimodal brain development study," *IEEE Transactions on Biomedical Engineering*, pp. 1–1, 2019.
- [15] R. Zhang, J. Li, H. Sun, Y. Ge, P. Luo, X. Wang, and L. Lin, "Scan: Self-and-collaborative attention network for video person re-identification," *IEEE Transactions on Image Processing*, pp. 1–1, 2019.
- [16] J. Liu, Y. Wang, Y. Li, J. Fu, J. Li, and H. Lu, "Collaborative deconvolutional neural networks for joint depth estimation and semantic segmentation," *IEEE Transactions on Neural Networks and Learning* Systems, vol. 29, no. 11, pp. 5655–5666, Nov 2018.
- [17] M. Zhu, J. Li, N. Wang, and X. Gao, "A deep collaborative framework for face photo-sketch synthesis," *IEEE Transactions on Neural Networks* and Learning Systems, pp. 1–13, 2019.
- [18] Z. Li, J. Tang, and T. Mei, "Deep collaborative embedding for social image understanding," *IEEE Transactions on Pattern Analysis and Machine Intelligence*, pp. 1–1, 2018.
- [19] Y. Xie, Y. Xia, J. Zhang, Y. Song, D. Feng, M. Fulham, and W. Cai, "Knowledge-based collaborative deep learning for benign-malignant lung nodule classification on chest ct," *IEEE Transactions on Medical Imaging*, vol. 38, no. 4, pp. 991–1004, April 2019.
- [20] M. Fu, H. Qu, Z. Yi, L. Lu, and Y. Liu, "A novel deep learning-based collaborative filtering model for recommendation system," *IEEE Transactions on Cybernetics*, vol. 49, no. 3, pp. 1084–1096, March 2019.
- [21] D. Chae, J. A. Shin, and S. Kim, "Collaborative adversarial autoencoders: An effective collaborative filtering model under the gan framework," *IEEE Access*, vol. 7, pp. 37 650–37 663, 2019.
- [22] X. Zeng, Y. Lin, Y. He, L. Lv, X. Min, and A. Rodrłguez-Paton, "Deep collaborative filtering for prediction of disease genes," *IEEE/ACM Transactions on Computational Biology and Bioinformatics*, pp. 1–1, 2019
- [23] H. Yue, J. Liu, J. Yang, T. Nguyen, and F. Wu, "High iso jpeg image denoising by deep fusion of collaborative and convolutional filtering," *IEEE Transactions on Image Processing*, pp. 1–1, 2019.
- [24] G. Hinton and T. Sejnowski, "Learning and releaming in boltzmann machines," Parallel distributed processing: Explorations in the microstructure of cognition, vol. 1, pp. 282–317, 1986.

- [25] G. E. Hinton, "Training products of experts by minimizing contrastive divergence," *Neural Computation*, vol. 14, no. 8, pp. 1771–1800, 2002.
- [26] M. A. Carreira-Perpinan and G. E. Hinton, "On contrastive divergence learning," in *Proceedings of the Tenth International Workshop on Arti*ficial Intelligence and Statistics. Citeseer, 2005, pp. 33–40.
- [27] S. Osindero and G. E. Hinton, "Modeling image patches with a directed hierarchy of markov random fields," in *Advances in Neural Information Processing Systems*, 2008, pp. 1121–1128.
- [28] I. Sutskever and G. E. Hinton, "Learning multilevel distributed representations for high-dimensional sequences," in *International Conference on Artificial Intelligence and Statistics*, 2007, pp. 548–555.
- [29] A. Courville, G. Desjardins, J. Bergstra, and Y. Bengio, "The spike-and-slab rbm and extensions to discrete and sparse data distributions," *IEEE Transactions on Pattern Analysis and Machine Intelligence*, vol. 36, no. 9, pp. 1874–1887, 2014.
- [30] C. Chen, C. Y. Zhang, L. Chen, and M. Gan, "Fuzzy restricted boltzmann machine for the enhancement of deep learning," *IEEE Transactions on Fuzzy Systems*, vol. 23, no. 6, pp. 2163–2173, 2015.
- [31] Z. Han, Z. Liu, J. Han, C.-M. Vong, S. Bu, and X. Li, "Unsupervised 3d local feature learning by circle convolutional restricted boltzmann machine," *IEEE Transactions on Image Processing*, vol. 25, no. 11, pp. 5331–5344, 2016.
- [32] J. Chu, H. Wang, H. Meng, P. Jin, and T. Li, "Restricted boltzmann machines with gaussian visible units guided by pairwise constraints," *IEEE Transactions on Cybernetics*, pp. 1–14, 2018.
- [33] J. Chu, T. Li, H. Wang, J. Liu, and M. Hua, "Self-learning local supervision encoding framework to constrict and disperse feature distribution for clustering," arXiv preprint arXiv:1812.01967, 2018.
- [34] C. L. P. Chen and S. Feng, "Generative and discriminative fuzzy restricted boltzmann machine learning for text and image classification," *IEEE Transactions on Cybernetics*, pp. 1–12, 2018.
- [35] D. Chen, J. Lv, and Z. Yi, "Graph regularized restricted boltzmann machine," *IEEE Transactions on Neural Networks and Learning Systems*, vol. 29, no. 6, pp. 2651–2659, June 2018.

- [36] S. Wang, Z. Zheng, S. Yin, J. Yang, and Q. Ji, "A novel dynamic model capturing spatial and temporal patterns for facial expression analysis," *IEEE Transactions on Pattern Analysis and Machine Intelligence*, pp. 1–1, 2019.
- [37] G. E. Hinton and R. R. Salakhutdinov, "Reducing the dimensionality of data with neural networks," *Science*, vol. 313, no. 5786, pp. 504–507, 2006
- [38] R. Salakhutdinov and G. Hinton, "An efficient learning procedure for deep boltzmann machines," *Neural Computation*, vol. 24, no. 8, pp. 1967–2006, 2012.
- [39] G. E. Hinton, S. Osindero, and Y.-W. Teh, "A fast learning algorithm for deep belief nets," *Neural Computation*, vol. 18, no. 7, pp. 1527–1554, 2006
- [40] K. H. Cho, T. Raiko, and A. Ilin, "Gaussian-bernoulli deep boltzmann machine," in the 2013 International Joint Conference on Neural Networks. IEEE, 2013, pp. 1–7.
- [41] J. Zhang, G. Tian, Y. Mu, and W. Fan, "Supervised deep learning with auxiliary networks," in the 20th ACM SIGKDD International Conference on Knowledge Discovery and Data Mining. ACM, 2014, pp. 353–361.
- [42] Y. Sun, X. Wang, and X. Tang, "Hybrid deep learning for face verification," *IEEE Transactions on Pattern Analysis and Machine Intelligence*, vol. 38, no. 10, pp. 1997–2009, Oct 2016.
- [43] L. Kim, "Deepx: Deep learning accelerator for restricted boltzmann machine artificial neural networks," *IEEE Transactions on Neural Networks* and Learning Systems, vol. 29, no. 5, pp. 1441–1453, May 2018.
- [44] L. Gu, J. Huang, and L. Yang, "On the representational power of restricted boltzmann machines for symmetric functions and boolean functions," *IEEE Transactions on Neural Networks and Learning Sys*tems, vol. 30, no. 5, pp. 1335–1347, May 2019.
- [45] F. O. D. Fran?a, "A hash-based co-clustering algorithm for categorical data," Expert Systems with Applications, vol. 64, pp. 24–35, 2016.
- [46] A. Banerjee, S. Merugu, I. S. Dhillon, and J. Ghosh, "Clustering with bregman divergences," *Journal of Machine Learning Research*, vol. 6, no. 4, pp. 1705–1749, 2005.
- [47] "Twcc: Automated two-way subspace weighting partitional coclustering," *Pattern Recognition*, vol. 76, pp. 404 – 415, 2018.
- [48] H. Li, M. Wang, and X.-S. Hua, "Msra-mm 2.0: A large-scale web multimedia dataset," in *IEEE International Conference on Data Mining Workshops*. IEEE, 2009, pp. 164–169.
- [49] D. Cai, X. He, and J. Han, "Document clustering using locality preserving indexing," *IEEE Transactions on Knowledge and Data Engineering*, vol. 17, no. 12, pp. 1624–1637, 2005.
- [50] F. O. de Fran?a, "A hash-based co-clustering algorithm for categorical data," Expert Systems with Applications, vol. 64, pp. 24 – 35, 2016.
- [51] R. Liu, H. Wang, and X. Yu, "Shared-nearest-neighbor-based clustering by fast search and find of density peaks," *Information Sciences*, vol. 450, pp. 200 – 226, 2018.
- [52] S. Lloyd, "Least squares quantization in pcm," *IEEE Transactions on Information Theory*, vol. 28, no. 2, pp. 129–137, 1982.
 [53] A. Y. Ng, M. I. Jordan, Y. Weiss *et al.*, "On spectral clustering: Analysis
- [53] A. Y. Ng, M. I. Jordan, Y. Weiss et al., "On spectral clustering: Analysis and an algorithm," Advances in Neural Information Processing Systems, vol. 2, pp. 849–856, 2002.



Hongjun Wang received his Ph.D. degree in computer science from Sichuan University of China in 2009. He is currently Associate Professor of the Key Lab of Cloud Computing and Intelligent Techniques in Southwest Jiaotong University. His research interests include machine learning, data mining and ensemble learning. He published over 30 research papers in journals and conferences and he is a member of ACM and CCF. He has a reviewer for several academic journals.



Jing Liu received his Ph.D. degree in management from Southwest Jiaotong University.She is currently an Assistant Professor of Business SchoolinSichuan University. Her research interests include machine learning, financial technology and modelling and forecasting high-frequency data.



Zeng Yu received the BS and MS degrees from the School of Mathematics, China University of Mining and Technology in 2008 and 2011, and the PhD degree from the School of Information Science and Technology, Southwest Jiaotong University in 2018, respectively. He was a visiting PhD student with Georgia State University, USA, from 2014 to 2016. He is currently an Assistant Professor in the School of Information Science and Technology, Southwest Jiaotong University. His research interests include data mining and deep learning.



Jielei Chu received the B.S. degree from Southwest Jiaotong University, Chengdu, China in 2008, and is currently working toward the Ph.D. degree at Southwest Jiaotong University. His research interests include deep learning, big data, semi-supervised learning and ensemble learning. He is a member of IEEE and CCF.



Tianrui Li (SM'11) received the B.S., M.S., and Ph.D. degrees in traffic information processing and control from Southwest Jiaotong University, Chengdu, China, in 1992, 1995, and 2002, respectively. He was a Post-Doctoral Researcher with Belgian Nuclear Research Centre, Mol, Belgium, from 2005 to 2006, and a Visiting Professor with Hasselt University, Hasselt, Belgium, in 2008; University of Technology, Sydney, Australia, in 2009; and University of Regina, Regina, Canada, in 2014. He is currently a Professor and the Director of the

Key Laboratory of Cloud Computing and Intelligent Techniques, Southwest Jiaotong University. He has authored or co-authored over 150 research papers in refereed journals and conferences. His research interests include big data, cloud computing, data mining, granular computing, and rough sets. Dr. Li is a fellow of the International Rough Set Society.